Carbohydrate Polymers 85 (2011) 824–831

Contents lists available at ScienceDirect

Carbohydrate Polymers

journal homepage: www.elsevier.com/locate/carbpol

Effects of starch nanocrystals on structure and properties of waterborne polyurethane-based composites

Jingwei Zou[a,1], Fang Zhang[b,1], Jin Huang[a,e,*], Peter R. Chang[c,**], Zhongmin Su[b], Jiahui Yu[d]

[a] College of Chemical Engineering, Wuhan University of Technology, Wuhan 430070, PR China
[b] Institute of Functional Material Chemistry, Faculty of Chemistry, Northeast Normal University, Changchun 130024, PR China
[c] Bioproducts and Bioprocesses National Science Program, Agriculture and Agri-Food Canada, 107 Science Place, Saskatoon, SK S7N 0X2, Canada
[d] Interdisciplinary Science and Technology Institute for Advanced Study, East China Normal University, Shanghai 200062, PR China
[e] State Key Laboratory of Pulp and Paper Engineering, South China University of Technology, Guangzhou 510640, PR China

ARTICLE INFO

Article history:
Received 19 January 2011
Received in revised form 8 March 2011
Accepted 1 April 2011
Available online 12 April 2011

Keywords:
Nanocomposite
Waterborne polyurethane
Starch nanocrystal

ABSTRACT

Starch nanocrystals (StN), which possesses a distinct platelet-like structure similar to exfoliated layered silicate, was incorporated into waterborne polyurethane (WPU) matrix at high loading levels to prepare WPU/StN nanocomposites. In our previous report (Chen et al., 2008a), the StN loading level was restricted to lower than 8 wt.% because self-aggregation of StN resulted in its sedimentation during preparation. However, in this work, good dispersion of the StN nanophase in the nanocomposites was observed even when the StN loading level reached 30 wt.%. Furthermore, the resultant composites exhibited prominent enhancement in both strength and Young's modulus, and maintained an elongation of greater than ca. 300%. A StN loading level of 10 wt.% showed the maximum tensile strength (31.1 MPa) and an enhanced Young's modulus, respectively ca.1.8- and 35.7-fold over those of neat WPU. The active surface and rigidity of StN facilitated formation of an interface for stress transfer and contributed to higher stress-endurance. As the StN loading level increased, self-aggregation of StNs resulted in a decrease in strength; however, the rigidity of StN supported an increase in Young's modulus, which was highest in nanocomposites containing 30 wt.% StNs. High performance waterborne polyurethane-based "green" bionanocomposites were thereby established.

Crown Copyright © 2011 Published by Elsevier Ltd. All rights reserved.

1. Introduction

Starch is a natural, renewable, and biodegradable polymer produced by many plants as a source of stored energy. Worldwide, the main sources of starch are maize, wheat, potatoes, cassava, rice, and legumes (Le Corre, Bras, & Dufresne, 2010). Starch nanocrystals (StNs) have been prepared by acid hydrolysis of starch granules followed by washing with successive centrifugation to produce a precipitate of starch nanocrystals. Conservation of the nanocrystals by freeze-drying converts the starch nanocrystals into a powder form. The freeze-dried starch nanocrystals stacked loosely in a fractal-like porous structure with a specific surface area of 3.23 m^2/g, much lower than that of perfectly individualized nanocrystals that were ca. 230 m^2/g, and higher than that of compact spherical aggregates (Angellier, Molina-Boisseau, & Dufresne, 2005; Chang, Huang, & Lin, 2011). The packing (and therefore surface area) of aggregates was also affected by differences in relative humidity during storage (Thielemans, Belgacem, & Dufresne, 2006). Availability of reactive hydroxyl groups on the surface of the freeze-dried powders was essential for chemical modification of the starch nanocrystals. The intrinsic rigidity of the nanocrystals, the special platelet-like morphology, the strong interfacial interactions, and the organization of the percolation network all contribute to optimized mechanical performance, thermal properties, solvent absorption, and barrier properties (Lin, Huang, Chang, Anderson, & Yu, 2011). Nanocomposites show unique properties compared to conventional composites because of the nanometric size effect, even with low filler content (Bondeson, Mathew, & Oksman, 2006). Nanocomposites have attracted much attention in the fields of academic research and practical application due to the reinforcing function of the incorporated nanoscale fillers, as well as their contributions to electronic, magnetic, and optical properties. Born out of the growing interest in nanocomposites and the focus on environmental friendliness, novel nanomaterials derived from biomass, known as "green" bio-nanocomposites, have been developed in which the biomass acts as the matrix, the nanofiller, or both.

* Corresponding author at: College of Chemical Engineering, Wuhan University of Technology, 122 Loushi Road, Wuhan 430070, China. Tel.: +86 27 87850343; fax: +86 27 87859019.
** Corresponding author.
E-mail addresses: huangjin@iccas.ac.cn (J. Huang), peter.chang@agr.gc.ca (P.R. Chang).
[1] These two authors have equivalent contribution to this work.

0144-8617/$ – see front matter Crown Copyright © 2011 Published by Elsevier Ltd. All rights reserved.
doi:10.1016/j.carbpol.2011.04.006

Among the components of bio-nanocomposites, the nanometer sized biofillers from biomass show unique advantages over traditional inorganic nanoparticles by virtue of their biodegradability and biocompatibility.

Starch nanocrystals have been compounded with many different kinds of polymer matrices. Using PVA as a matrix, Chen, Cao, Chang, and Huneault (2008) reported a low reinforcing effect and a slight improvement to properties when the pea starch nanocrystal content was lower than 10 wt.%, and a decrease in both the elongation at break and strength when the nanocrystal content was higher than 10 wt.%. Zheng, Ai, Chang, Huang, and Dufresne (2009) reported an increase in strength and Young's modulus, together with a decrease in elongation at break, at low pea starch nanocrystal loading levels (lower than 2 wt.%) in a soy protein isolate (SPI) matrix, which was attributed to uniform dispersion of the nanocrystals. Another interesting phenomenon reported in some composites is the observation of a constant elongation at break with increasing filler content. Indeed, Wang and Zhang (2008) reported the preparation of a high-strength WPU-based elastomer reinforced with 1–5% waxy maize starch nanocrystals. Low filler content allowed better dispersion of the StNs in the WPU matrix, allowing stronger interactions.

Waterborne polyurethane (WPU) is regarded as a nontoxic, non-flammable, and biodegradable material (Wicks, Wicks, & Rosthauser, 2002; Noble, 1997). Environmentally friendly WPU can be applied to leather and textile finishing, floor coverings, adhesives, pressure sensitive adhesives, and so on (Brinkman and Vandevoorde, 1997; Coogan, 1997; Duecoffre, Diener, Flosbach, & Schubert, 1997; Kim, Kim, & Jeong, 1994; Lin and Hsieh, 1997). Starch (Wu and Zhang, 2001), soy protein (Wang and Zhang, 2005), and lignin (Cui, Xia, Chen, Wei, & Huang, 2007) have been incorporated into WPU for the purposes of reducing cost, improving biodegradability, and enhancing mechanical performance. High loading levels of cellulose whisker have been filled into a WPU matrix as the reinforcing nanophase resulting in a significant increase in strength and Young's modulus (Cao, Dong, & Li, 2007). The effects of low levels of starch nanocrystal in modifying waterborne polyurethane have been studied in our previous works (Chen et al., 2008a). An interesting and innovative approach in the use of nanocrystals as fillers is the investigation of a synergistic reinforcement of waterborne polyurethane by both starch nanocrystals and cellulose whiskers (Wang, Tian, & Zhang, 2010). The authors reported that a system of WPU/1% StN/0.4% cellulose whiskers exhibited a much better reinforcing effect than all other tested WPU/StN and WPU/cellulose whiskers composites. The distinct platelet-like structure of starch nanocrystal as well as its rigidity, which is similar to that of exfoliated layered silicate (Jiang, Zhang, & Wolcott, 2007; Yu et al., 2007), produced extraordinary mechanical performance even at the low levels introduced into the polymer matrix. Self-aggregation starch nanocrystals was quite noticeably during its preparation (Zhang et al., 2010). We speculate that starch nanocrystal added in high levels could/would have some benefits in nanocomposites as well as expand the utilization of renewable biomass. High loading levels (30%) of starch nanocrystal have been incorporated as the reinforcing filler into natural rubber (Angellier, Molina-Boisseau, & Dufresne, 2005; Le Corre et al., 2009) and thermoplastic starch (Angellier, Molina-Boisseau, Dole, & Dufresne, 2006), resulting in a significant enhancement of strength and modulus. We strongly believe that inhibition of aggregation in aqueous solution and control of starch nanocrystal dispersion in the matrix can be realized to utilize this bioresource fully and to enhance of nanocomposites.

In this work, we inhibited the sedimentation and self-aggregation of starch nanocrystals. High levels of StNs were incorporated into WPU to prepare WPU/StN nanocomposites. The structure and mechanical properties of the resultant nanocomposite materials were investigated by attenuated total reflection-Fourier transform infrared spectroscopy (ATR-FTIR), X-ray diffraction (XRD), differential scanning calorimetry (DSC), dynamic mechanical analysis (DMA), scanning electron microscopy (SEM), and tensile testing. We are thereby pleased to report excellent enhancement of composites with high loading levels of StN.

2. Experimental

2.1. Materials

Pea starch, with an average granule size of 30 μm and composed of 35 wt.% amylose and 65 wt.% amylopectin, was supplied by Nutri-Pea Ltd. (Portage la Prairie, Canada). Polycaprolactone, with a number-average molecular weight (Mn) of 2000 (PCL_{2000}), was purchased from Sigma–Aldrich Co. (Saint Louis, MO, USA). Diphenyl-methane-diisocyanate (MDI-100) was purchased from Yantai Wanhua Polyurethanes Co. Ltd. (Shandong, China). Dimethylol propionic acid (DMPA) was donated by Huzhou Changsheng Chemical Co. Ltd. (Zhejiang, China), and dehydrated under vacuum at 60 °C for 12 h. Triethylamine (TEA) was purchased from Sinopharm Chemical Reagent Co. Ltd. (Shanghai, China), and redistilled before use. Analytical grade butanone was purchased from Sinopharm Chemical Reagent Co. Ltd. (Shanghai, China) and dehydrated by adding CaH_2 and then distilling.

2.2. Preparation of starch nanocrystals

According to the method of a previous report (Angellier, Choisnard, Molina-Boisseau, Ozil, & Dufresne, 2004), 36.725 g of pea starch was dispersed in 250 mL of 3.16 M H_2SO_4 aqueous solution, and stirred at a speed of 100 rpm for five days at 40 °C. Subsequently, the crude suspension containing starch nanocrystals (StNs) was centrifuged and then washed repeatedly with distilled water until the pH approached 7.0. Finally, for TEM observation the StN precipitate was homogenized ultrasonically in an aqueous solution for 3 min using a JY92-2D ultrasonic instrument (Ningbo Scientz Biotechnology Co. Ltd., China). The TEM image of StNs is shown in Fig. 1. Although the StNs tended to self-aggregate, isolated StNs were observed to have a width of 15–20 nm and a length of 40–70 nm.

2.3. Preparation of WPU/StN nanocomposites

The synthesis of waterborne polyurethane (WPU) is depicted as follows: Both 4.98 g PCL_{2000} and 2.23 g MDI were first dissolved in 10 g butanone and then placed in a three-necked round-bottom flask equipped with a mechanical stirrer, a reflux condenser, and a dry nitrogen inlet. The reactant was then heated to ca.70 °C, and kept under a nitrogen atmosphere for 2 h with mechanical stirring. Thereafter, 0.46 g DMPA, a chain-extender, was dispersed in butanone and added to give a NCO/OH molar ratio of 1.6. The reaction temperature was elevated to 85 °C and held for 1 h, during which time butanone was occasionally added in order to lower the viscidity of the reactant. Afterward, the resultant product was cooled to below 40 °C, and the –COOH of DMPA in the polyurethane chains neutralized by adding 0.34 g TEA. Emulsification was subsequently carried out by adding icy water under severe shear to produce WPU latex with a solids content of 20 wt.%.

The procedure for preparing homogeneous StN slurry is briefly stated as follows: a certain amount of StN was added to a calculated amount of water and stirred for half an hour. Thereafter, the mixture was dispersed ultrasonically for 1 h at 25 °C to obtain a uniform emulsion.

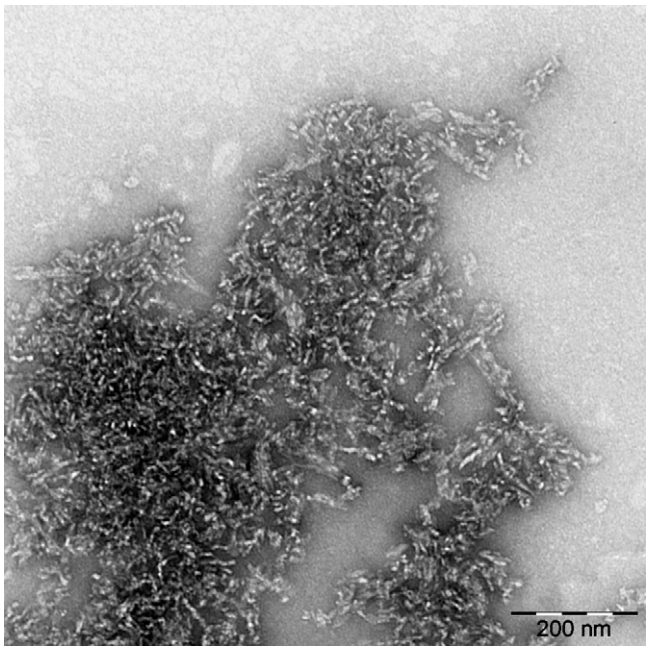

Fig. 1. TEM image of negatively stained pea starch nanocrystals.

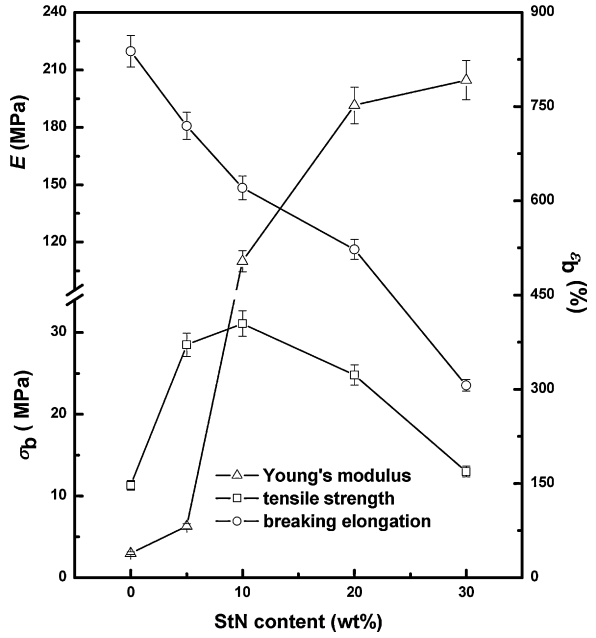

Fig. 2. Effects of StN loading level on tensile strength (σ_b), elongation at break (ε_b) and Young's modulus (E) of WPU/StN nanocomposite films, with WPU film as reference.

The uniform StN emulsion was added to WPU latex and allowed to continue stirring for another 0.5 h. The WPU latex was cast on a Teflon mold after vacuum degassing, and allowed to solidify as a film at 60 °C via water evaporation. The thickness of the resultant films was determined to be about 200 μm. By changing the StN content to 0, 5, 10, 20, and 30 wt.%, a series of nanocomposite films was obtained and coded as WPU, WPU/StN-5, WPU/StN-10, WPU/StN-20, and WPU/StN-30, respectively. The films were stored at room temperature in a desiccator containing P_2O_5 with 0% relative humidity (RH) for 5 days.

2.4. Characterization

Attenuated total reflectance-Fourier transform infrared (ATR-FTIR) spectra of all the films were recorded on a FTIR 5700 spectrometer (Nicolet, USA). The films were scanned in the range of 4000–700 cm^{-1} using Smart OMNT reflect accessories.

X-ray diffraction (XRD) measurements were performed on a D/max-IIIA X-ray diffractometer (Rigaku Denki, Tokyo, Japan) using Cu K_α radiation (λ = 0.154 nm) at 40 kV and 60 mA with a scan rate of 12° min^{-1}. The diffraction angle of 2θ ranged from 3° to 60°.

TEM photographs of StNs were taken with an H-7000FA transmission electron microscope (Hitachi, Japan) at an acceleration voltage of 75 kV. Deposited StNs were negatively stained with an aqueous 2% solution of uranyl acetate before observation.

Scanning electron microscope (SEM) observation was carried out on an S-4800 scanning electron microscope (Hitachi, Japan) with an accelerating voltage of 5 kV. The films were frozen in liquid nitrogen and then immediately snapped. The fracture surfaces were sputtered with Pt, then observed and photographed.

Differential scanning calorimetry (DSC) was carried out on a DSC-204 instrument (Netzsch, Germany) under a nitrogen atmosphere at a heating or cooling rate of 20 °C min^{-1}. The specimen was scanned over a range of −150–100 °C after pre-treatment (heating from 20 °C to 100 °C and then cooling to −150 °C) to eliminate thermal history and remove volatiles.

Dynamic mechanical analysis (DMA) measurement was carried out on a DMA-242C dynamic mechanical analyzer (Netzsch, Germany) at a frequency of 1 Hz over a range of −150–100 °C with a heating rate of 3 °C min^{-1}. A dual cantilever device was used and the specimen size was 40 × 10 × ca. 0.5 mm^3.

The tensile strength (σ_b), elongation at break (ε_b) and Young's modulus (E) were measured on a CMT6503 universal testing machine (SANS, Shenzhen, China) with a crosshead rate of 100 mm min^{-1} according to method GB13022-91. The tested specimens were cut into quadrate strips 10 mm wide and the distance between testing marks was 30 mm. The average value of five replicates of each sample was taken.

3. Results and discussion

3.1. Mechanical properties of nanocomposites

Fig. 2 shows the effects of StN loading levels on the WPU/StN nanocomposite mechanical properties including tensile strength (σ_b), Young's modulus (E) and elongation at break (ε_b). As expected, the rigidity of StN significantly enhanced the strength of the WPU; compared with σ_b of 11.3 MPa and E of 3.0 MPa for neat WPU, the σ_b and E values of the WPU/StN nanocomposites were both enhanced. When the StN loading level was 10 wt.%, σ_b reached a maximum value of 31.1 MPa, approximately 1.8-fold over that of neat WPU; thereafter, increases in the StN loading level resulted in a decrease in σ_b, but the value of E continued to increase. When the StN loading level was 30 wt.%, E increased to 204.6 MPa, ca. 67.2-fold over that of neat WPU. The change in ε_b as the StN content increased was the opposite of E, and all the ε_b values for the WPU/StN nanocomposites were lower than that of neat WPU. In other words, enhancement of the strength and Young's modulus occurred at the expense of elongation; however, with the obvious enhancement of σ_b and E, a certain level of decline in ε_b is acceptable. From the above results, we found that neat StNs had an evident reinforcing role. Furthermore, with a StN content of 10 wt.%, σ_b reached its maximum value and E reached 110.1 MPa, ca. 1.8 and 35.7-fold, respectively, over those of neat WPU, while the ε_b value of the nanocomposites remained at 620.6%. Enhancement of the nanocomposite mechanical properties by StNs may be attributed to the uniform dispersion of StNs, as well as to the physical interaction between the StN filler

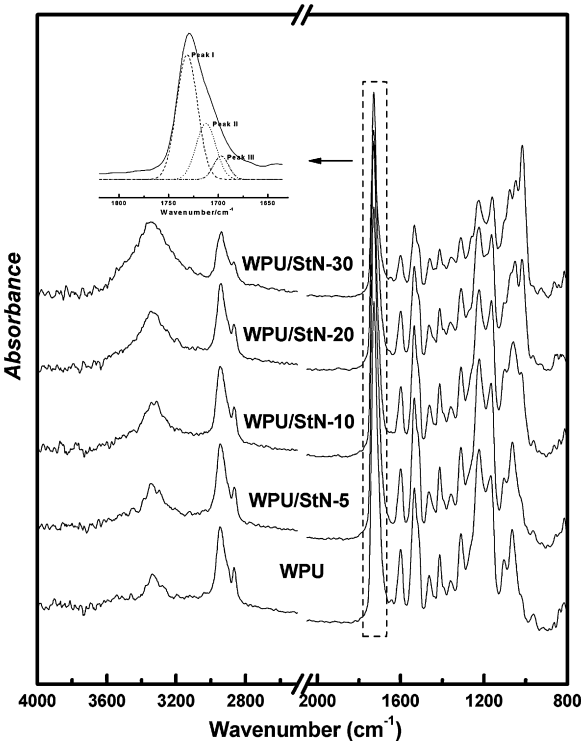

Fig. 3. Full ATR-FTIR spectra of WPU/StN nanocomposites and WPU film, as well as the curve-fitted FTIR spectra of WPU in the range of 1600–1800 cm^{-1} for reference. ((—) Experimental curve; (- - -) free –C=O; (. . .) –C=O in amorphous region; (– – –) –C=O in ordered domain).

and the WPU matrix (Kim, Fasulo, Rodgers, & Paul, 2007) that allows for the transfer of stress to the rigid nanofiller. With an increase in the StN loading level, however, self-aggregation of StNs may break the original structure and interactions of the WPU matrix, resulting in a decrease in strength and elongation. Nevertheless, the rigid nature of StN and its aggregate maintained the continuous increase in Young's modulus.

3.2. Hydrogen bonding in nanocomposites

ATR-FTIR spectra of the WPU/StN nanocomposites and the neat WPU are shown in Fig. 3. The hydrogen bond is an essential physical interaction in waterborne polyurethane that affects the microphase separation structure and mechanical properties of materials. In this case, the –NH in the hard-segment was hydrogen-bonded with the –C=O of the hard-segments and with the ester –C=O of the PCL_{2000} soft-segments. In addition, –OH on the StN surface participated in hydrogen bonding with the –C=O in the soft- and hard-segments. The analogical –C=O bands of the WPU/StN nanocomposites and of WPU were divided into three peaks, namely Peak I from the free –C=O located at 1730–1732 cm^{-1}, Peak II from the hydrogen-bonded –C=O in the amorphous region located at 1712–1713 cm^{-1}, and Peak III from the hydrogen-bonded –C=O in the ordered domain located at 1697–1698 cm^{-1} (Huang and Zhang, 2002). The locations and fractions of these three peaks in the WPU/StN nanocomposites and WPU are summarized in Table 1. Adding StNs appeared to slightly decrease the fraction of the free –C=O peak (Peak I), indicating that the hydrogen bonding associated with –C=O of hard-segments and PCL_{2000} soft-segments was improved. This was attributed to the newly formed hydrogen bonds between the –C=O of the WPU component and the –OH on the StN surface. Although hydrogen bonding associated with –C=O improved as a whole, the effect of adding StN on the region of hydrogen bonding in the nanocomposites was distinctly different. With

Table 1
Locations and fractions of curve-fitting peaks for the –C=O bands in the FTIR spectra of the WPU/StN nanocomposites and WPU (Peak I: free –C=O; Peak II: hydrogen-bonded –C=O in amorphous region; Peak III: hydrogen-bonded –C=O in ordered domain).

Sample	Peak I[a]		Peak II		Peak III	
	Location (cm^{-1})	Fraction (%)	Location (cm^{-1})	Fraction (%)	Location (cm^{-1})	Fraction (%)
WPU	1731.5	65.2	1712.4	24.1	1697.3	10.7
WPU/StN-5	1730.2	64.5	1712.4	25.2	1697.5	10.3
WPU/StN-10	1730.8	63.8	1712.9	25.6	1697.1	10.6
WPU/StN-20	1731.7	62.5	1712.2	28.1	1697.1	9.4
WPU/StN-30	1731.7	61.6	1712.4	29.5	1697.5	8.9

[a] Peak I, free –C=O; Peak II, hydrogen-bonded –C=O in amorphous region; Peak III, hydrogen-bonded –C=O in ordered domain.

an increase in the StN loading level, the increasing fraction of Peak II suggested that improved hydrogen bonding occurred mainly in the amorphous region, while the slight decrease in the fraction of Peak III proved the cleavage of hydrogen bonding in the ordered domain. Hydrogen bonding in the ordered domain was usually constructed by hard-segments in the WPU matrix, suggesting that adding StN demolished the original ordered alignment of hard-segments.

3.3. Crystalline character of nanocomposites

Fig. 4 shows the XRD patterns of the WPU/StN nanocomposites with various StN loading levels, as well as those of neat WPU and StN. The WPU showed a diffuse peak located at 20.1° of 2θ, in spite of the fact that –C=O-based hydrogen bonds constructed a small scale ordered domain in the WPU matrix, as mentioned above. Because the StNs were semi-crystalline, well-defined diffraction peaks appeared in the WPU/StN nanocomposites. The diffraction peak located at 23.6° of 2θ, corresponded to the diffraction peak of StN located at 22.9° of 2θ, present in all nanocomposites. This suggested that the crystalline character of StN existed in the

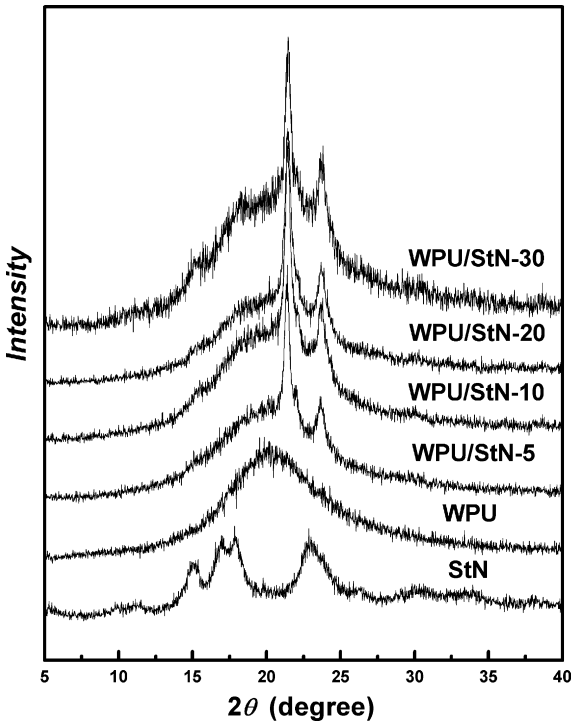

Fig. 4. XRD patterns of WPU/StN nanocomposites as well as WPU film and freeze-dried StN powder.

Table 2
DSC and DMA data for WPU/StN nanocomposites with WPU film as reference.

Sample	DSC Data				DMA Data			
	$T_{g,mid}$ (°C)	ΔC_p (J g^{-1} K^{-1})	T_m (°C)	ΔH_m (J g^{-1})	$T_{\alpha,onset}$ (°C)	log E' (MPa)	$T_{\alpha,max}$ (°C)	tan δ
WPU	−46.7	−0.19	45.2	2.34	−50.6	3.29	−33.1	0.22
WPU/StN-5	−46.4	−0.15	45.2	5.51	−49.7	3.31	−32.2	0.23
WPU/StN-10	−46.0	−0.13	46.5	8.29	−49.6	3.38	−32.0	0.19
WPU/StN-20	−45.9	−0.14	47.3	8.89	−49.0	3.38	−30.6	0.22
WPU/StN-30	−45.4	−0.22	47.4	12.50	−48.5	3.41	−30.5	0.25

nanocomposites. However, the other typical diffraction peaks of StN located at 15.0° and 17.9° of 2θ were shielded by the diffuse diffraction of WPU matrix. Only two weak diffraction peaks located at 15.2° and 18.3° of 2θ could be identified until the StN loading level increased up to 30 wt.%. With the introduction of StNs into WPU, the most obvious change was a new strong peak that presented at 21.4° of 2θ, and did not correspond to any peaks in the diffraction of StN. This may be attributed to the presence of StNs changing and improving the crystalline character of WPU.

3.4. Thermal behaviour of nanocomposites

DSC and DMA were used to further understand the interaction between the StN filler and the WPU matrix, associated with the structural changes of WPU matrix and the distribution of StN filler, by observing variances in the domain-scale glass transition and the molecular level α-relaxation assigned to the PCL_{2000} soft-segment, respectively. Fig. 5(A) shows the DSC thermograms of the WPU/StN nanocomposites and neat WPU. The data for the glass transition temperature at midpoint ($T_{g,mid}$), the heat-capacity increment (ΔC_p), the melting temperature (T_m), and the heat enthalpy (ΔH_m) are listed in Table 2. In the WPU/StN nanocomposites, the temperatures for glass transition (T_g) and α-relaxation (T_α) of the PCL_{2000} soft-segment can be affected by StNs in two opposite ways. First, the motion of the soft-segment may be suppressed by the steric hindrance of the rigid StN nanophase and by hydrogen bonding on the active StN surface resulting in T_g and T_α shifting to a higher temperature. In the opposite way, incorporating StNs may cleave the original interaction between the hard- and soft-segments and hence change the microphase structure in the WPU matrix. In other words, the soft-segment could escape the binding of the hard-segment, leading to decreased T_g and T_α. The $T_{g,mid}$s of all the WPU/StN nanocomposites were higher than that of neat WPU, suggesting that restriction of the mobility of soft-segments by StNs was dominant in spite of the inevitable cleavage of the original interaction between the hard- and soft-segments in the WPU matrix. Even when the StN content was high and StNs aggregated into small particles, they could still disperse homogeneously in the WPU matrix and inhibit the motion of the soft-segment, mediated by the newly formed interaction with the WPU component. The $T_{g,mid}$s therefore increased with an increase in StN loading level. On the other hand, compared with the ΔH_m value of 2.34 J g^{-1} for the neat WPU, all WPU/StN nanocomposites showed dramatically higher ΔH_m values, suggesting that increasing the StN loading level improved the crystallinity of the PCL component in the WPU matrix due to the nucleation effect of the StN.

DMA is a powerful technique that reflects the mobility of the soft-segment through α-relaxation at the molecular level, for which the specific heat increment of the domain-scale glass transition, as measured by DSC, is generally ill-defined. Fig. 5(B) shows the logarithm of the storage modulus (log E') and the tangent of the loss angle (tan δ) as a function of temperature. The α-relaxation temperature at onset ($T_{\alpha,onset}$) and the corresponding storage modulus (log E'), α-relaxation temperature of loss peak ($T_{\alpha,onset}$), and the tangent of loss angle (tan δ) are summarized in Table 2. Obviously, the $T_{\alpha,max}$s of all the WPU/StN nanocomposites were higher than that of neat WPU. Considering the improved hydrogen bonding associated with –C=O in the amorphous region of the WPU matrix (seen

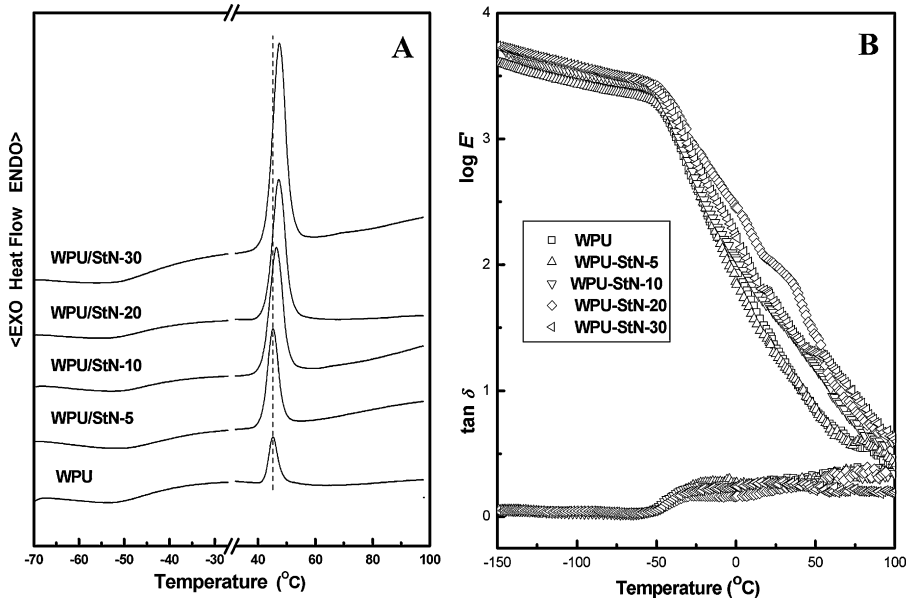

Fig. 5. (A) DSC thermograms of WPU/StN nanocomposites with WPU film as reference; (B) Logarithm of storage modulus (log E') and tangent of loss angle (tan δ) vs. temperature measured at 1 Hz for WPU/StN nanocomposites with various StN loading levels, and WPU film as reference.

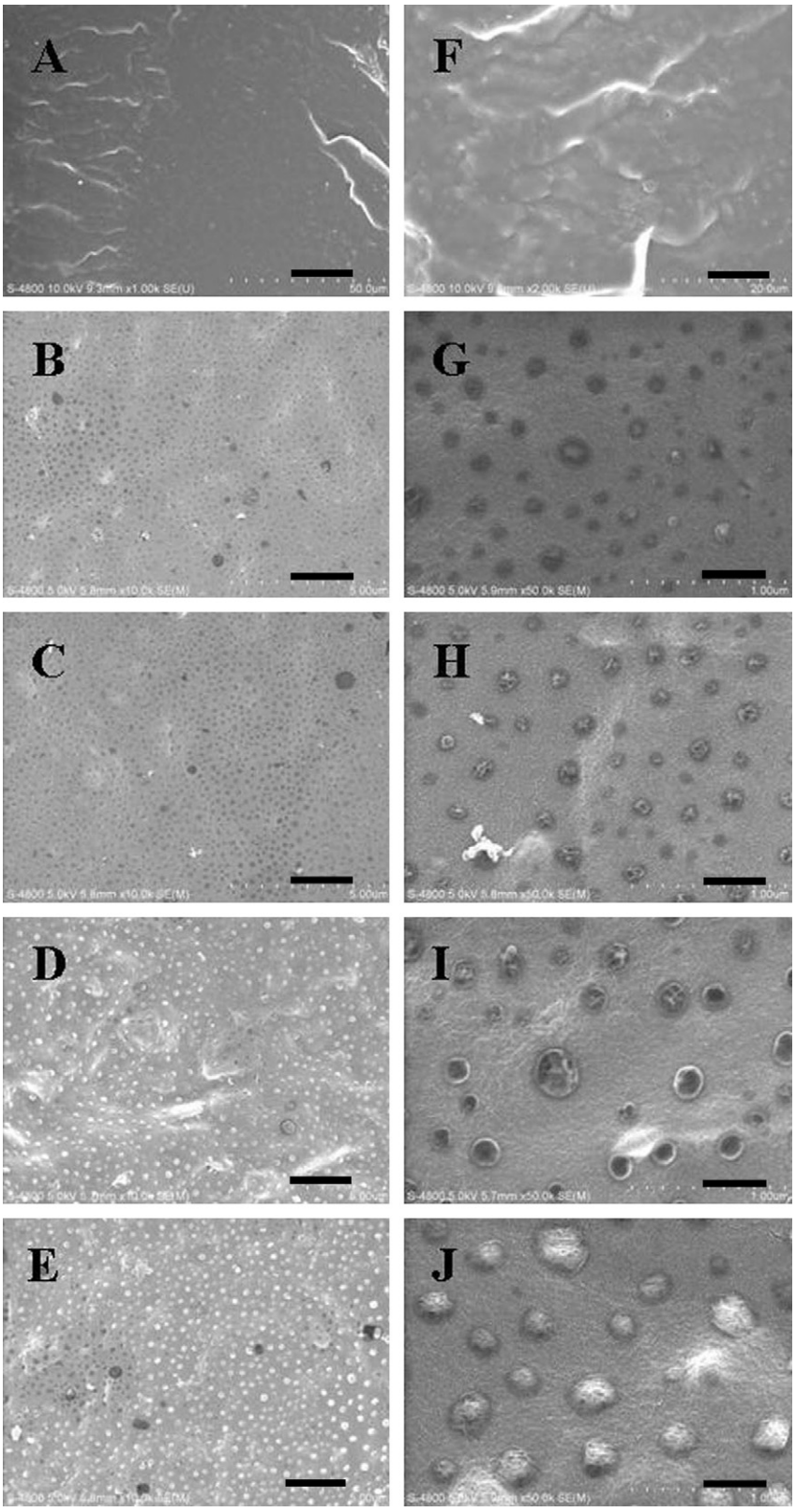

Fig. 6. SEM images of fractured surfaces of WPU/StN nanocomposites with various StN loading levels and WPU film reference. ((A) WPU, (B) WPU/StN-5, (C) WPU/StN-10, (D) WPU/StN-20, (E) WPU/StN-30; (F)–(J) are high multiple electron micrographs corresponding to (A)–(E). Scale bar: 20 μm in (A) and 10 μm in (F); 2 μm in (B)–(E); 400 nm in (G)–(J).)

in Table 1), the increase in $T_{\alpha,max}$s was attributed to the formation of interactions between the polar groups on the StN surface and the WPU matrix. In this case, the suppression of StNs to the mobility of soft-segments was proportional to the effective surface area of StNs. The increasing interfacial area between the StN filler and the WPU matrix resulted in an increase in $T_{\alpha,max}$s and $T_{\alpha,onset}$s with an increase in the StN loading level. This is in good agreement with the DSC results. In the WPU/StN nanocomposites, the StN nanophase filler (Cui, Ma, & Paul, 2007) and the ordered hard-segment domain of the WPU matrix were mainly responsible for the rigidity. Although the ordered hard-segment domain of the WPU matrix partly cleaved after the addition of StN (seen in Section 3 on the hydrogen bonding associated with –C=O in ordered domain), the log E' of all the WPU/StN nanocomposites were still higher than that of neat WPU due to the reinforcing function of rigid StN. This was in positive correlation with the Young's modulus (E) of the nanocomposites.

3.5. Fracture morphologies of nanocomposites

Fig. 6 shows the SEM images of fractured surfaces of the WPU/StN nanocomposites and neat WPU. Interestingly, WPU/StN nanocomposites show completely different fracture morphology as compared with neat WPU; however, in spite of varying StN contents, all the WPU/StN nanocomposites show similar fracture morphology. Nanoparticles are obviously present in the WPU/StN nanocomposites, and increasing the StN loading level caused the size of the nanoparticles to become larger and gradually to increase in number. This phenomenon was in agreement with the decrease in strength and elongation at break, and was attributed to breakage of the original structure of the WPU matrix after adding higher levels of StNs. In addition, the StN nanophase was observed to have dispersed well in the WPU matrix as the loading level increased. The SEM images seemed to verify the effects of increasing the StN loading level on the increasing number and expanded size of the StN nanophase in the nanocomposites.

4. Conclusions

Nanocomposite materials were prepared by casting and evaporating a mixture using waterborne polyurethane (WPU) as the matrix and starch nanocrystal (StN) as the filler. The strength and Young's modulus of the nanocomposites were simultaneously enhanced and ca. 300% elongation was maintained. Herein, the WPU/StN containing 10 wt.% StNs had the maximum tensile strength (31.1 MPa) and an enhanced Young's modulus (110.1 MPa) that were ca.1.8- and 35.7-fold over those of neat WPU, respectively. The WPU/StN containing 30 wt.% StNs had the highest Young's modulus (204.6 MPa), which was enhanced by ca. 6720%. The prominent improvement of mechanical performance was attributed to the enduring stress of the rigid StN and stress transfer mediated by strong interactions between the StN filler and the WPU matrix. This work rendered a strategy for achieving high mechanical performance of waterborne polyurethane-based nanocomposites by a simple method, and the novel bionanocomposites developed could have great potential applications.

Acknowledgements

This research work was financially supported by the National Natural Science Foundation of China (50873080); Program of Energy Research and Development (PERD) of Canada; Agricultural Bio-products Innovation Program (ABIP) of Canada via the Pulse Research Network (PURENET); Fundamental Research Funds for the Central Universities (Self-Determined and Innovative Research Funds of WUT 2010-II-022); and State Key Laboratory of Pulp and Paper Engineering (200906).

References

Angellier, H., Choisnard, L., Molina-Boisseau, S., Ozil, P., & Dufresne, A. (2004). Optimization of the preparation of aqueous suspensions of waxy maize starch nanocrystals using a response surface methodology. *Biomacromolecules*, *5*, 1545–1551.

Angellier, H., Molina-Boisseau, S., & Dufresne, A. (2005). Mechanical properties of waxy maize starch nanocrystal reinforced natural rubber. *Macromolecules*, *38*, 9161–9170.

Angellier, H., Molina-Boisseau, S., Lebrun, L., & Dufresne, A. (2005). Processing and structural properties of waxy maize starch nanocrystals reinforced natural rubber. *Macromolecules*, *38*, 3783–3792.

Angellier, H., Molina-Boisseau, S., Dole, P., & Dufresne, A. (2006). Thermoplastic starch-waxy maize starch nanocrystals nanocomposites. *Biomacromolecules*, *7*, 531–539.

Bondeson, D., Mathew, A., & Oksman, K. (2006). Optimization of the isolation of nanocrystals from microcrystalline cellulose by acid hydrolysis. *Cellulose*, *13*, 171–180.

Brinkman, E., & Vandevoorde, P. (1997). Waterborne two-pack isocyanate-free systems for industrial coatings. *Progress in Organic Coatings*, *34*, 21–25.

Cao, X. D., Dong, H., & Li, C. M. (2007). New nanocomposite materials reinforced with flax cellulose nanocrystals in waterborne polyurethane. *Biomacromolecules*, *8*, 899–904.

Chang, P. R., Huang, J., & Lin, N. (2011). Bio-nanocomposites with non-cellulosic biofillers. In V. Mittal (Ed.), *Nanocomposites with biodegradable polymers: synthesis, properties and future perspectives* (pp. 71–100). London: Oxford University Press.

Chen, G. J., Wei, M., Chen, J. H., Huang, J., Dufresne, A., & Chang, P. R. (2008). Simultaneous reinforcing and toughening: new nanocomposites of waterborne polyurethane filled with low loading level of starch nanocrystals. *Polymer*, *49*, 1860–1870.

Chen, Y., Cao, X., Chang, P. R., & Huneault, M. A. (2008). Comparative study on the films of poly (vinyl alcohol)/pea starch nanocrystals and poly (vinyl alcohol)/native pea starch. *Carbohydrate Polymers*, *73*, 8–17.

Coogan, R. G. (1997). Post-crosslinking of water-borne urethanes. *Progress in Organic Coatings*, *32*, 51–63.

Cui, G. J., Xia, W. B., Chen, G. J., Wei, M., & Huang, J. (2007). Enhanced mechanical performances of waterborne polyurethane loaded with lignosulfonate and its supramolecular complexes. *Journal of Applied Polymer Science*, *106*, 4257–4263.

Cui, L. L., Ma, X. Y., & Paul, D. R. (2007). Morphology and properties of nanocomposites formed from ethylene-vinyl acetate copolymers and organoclays. *Polymer*, *48*, 6325–6339.

Duecoffre, V., Diener, W., Flosbach, C., & Schubert, W. (1997). Emulsifiers with high chemical resistance: a key to high performance waterborne coatings. *Progress in Organic Coatings*, *34*, 200–205.

Huang, J., & Zhang, L. (2002). Effects of NCO/OH molar ratio on structure and properties of graft-interpenetrating polymer networks from polyurethane and nitrolignin. *Polymer*, *43*, 2287–2294.

Jiang, L., Zhang, J., & Wolcott, M. P. (2007). Comparison of polylactide/nano-sized calcium carbonate and polylactide/montmorillonite composites: Reinforcing effects and toughening mechanisms. *Polymer*, *48*, 7632–7644.

Kim, B. K., Kim, T. K., & Jeong, H. M. (1994). Aqueous dispersion of polyurethane anionomers from H_{12}MDI/IPDI, PCL, BD, and DMPA. *Journal of Applied Polymer Science*, *53*, 371–378.

Kim, D. H., Fasulo, P. D., Rodgers, W. R., & Paul, D. R. (2007). Effect of the ratio of maleated polypropylene to organoclay on the structure and properties of TPO-based nanocomposites. Part I. Morphology and mechanical properties. *Polymer*, *48*, 5960–5978.

Le Corre, D., Bras, J., & Dufresne, A. (2009). 2nd International Conference on Biodegradable Polymers and Sustainable Composites, (BIOPOL 2009), Alicante, Spain.

Le Corre, D., Bras, J., & Dufresne, A. (2010). Starch nanoparticles: A review. *Biomacromolecules*, *11*, 1139–1153.

Lin, N., Huang, J., Chang, P. R., Anderson, D. P., & Yu, J. H. (2011). Preparation, modification, and application of starch nanocrystals in nanomaterials: A review. *Journal of Nanomaterials*, 13 (2011, Article ID 573687).

Lin, Y., & Hsieh, F. (1997). Water-blown flexible polyurethane foam extender with biomass materials. *Journal of Applied Polymer Science*, *65*, 695–703.

Noble, K. L. (1997). Waterborne polyurethanes. *Progress in Organic Coatings*, *32*, 131–136.

Thielemans, W., Belgacem, M. N., & Dufresne, A. (2006). Starch nanocrystals with large chain surface modifications. *Langmuir*, *22*, 4804–4810.

Wang, N. G., & Zhang, L. N. (2005). Preparation and characterization of soy protein plastics plasticized with waterborne polyurethane. *Polymer International*, *54*, 233–239.

Wang, Y., & Zhang, L. (2008). High-strength waterborne polyurethane reinforced with waxy maize starch nanocrystals. *Journal of Nanoscience and Nanotechnology*, *8*, 5831–5838.

Wang, Y. X., Tian, H. F., & Zhang, L. (2010). Role of starch nanocrystals and cellulose whiskers in synergistic reinforcement of waterborne polyurethane. *Carbohydrate Polymers*, *80*, 665–671.

Wicks, Z. W., Wicks, D. A., & Rosthauser, J. W. (2002). Two package waterborne urethane systems. *Progress in Organic Coatings*, *44*, 161–183.

Wu, Q. X., & Zhang, L. N. (2001). Structure and properties of casting films blended with starch and waterborne polyurethane. *Journal of Applied Polymer Science*, *79*, 2006–2013.

Yu, Z., Yin, J., Yan, S., Xie, Y., Ma, J., & Chen, X. (2007). Biodegradable poly (L-lactide)/poly(ε-caprolactone)-modified montmorillonite nanocomposites: Preparation and characterization. *Polymer*, *48*, 6439–6447.

Zhang, X. L., Huang, J., Chang, P. R., Li, J. L., Chen, Y. M., Wang, D. X., Yu, J. H., & Chen, J. H. (2010). Structure and properties of polysaccharide nanocrystal-doped supramolecular hydrogels based on cyclodextrin inclusion. *Polymer*, *51*, 4398–4407.

Zheng, H., Ai, F., Chang, P. R., Huang, J., & Dufresne, A. (2009). Structure and properties of starch nanocrystal reinforced soy protein plastics. *Polymer Composites*, *30*, 474–480.